JOURNAL OF GEOPHYSICAL RESEARCH, VOL. 95, NO. C7, PAGES 11,575–11,590, JULY 15, 1990

The Spatial and Temporal Variability of Sand Bar Morphology

T. C. LIPPMANN AND R. A. HOLMAN

College of Oceanography, Oregon State University, Corvallis

The spatial and temporal variability of nearshore sand bar morphology is quantified using a unique data set spanning 2 years. The data consist of daily time exposure images of incident wave breaking on an open coast sandy beach which may be used to infer bar morphology (Lippmann and Holman, 1989). The morphology in each image is classified into an eight state morphologic scheme in which bars are uniquely defined by four independent criteria. The most frequently observed morphologies are the longshore-periodic (rhythmic) bars, observed in 68% of the data. Linear bars occur under highest wave conditions ($\bar{H}_s$ = 1.78 m) and are unstable (mean residence time ≈ 2 days). Shore-attached rhythmic bars are the most stable (mean residence time ≈ 11 days) and generally form 5–16 days following peak wave events. Non-rhythmic, three-dimensional bars are very transient (mean residence time ≈ 3 days). Eighty-seven percent of transitions to lower bar types (defined in text) occurred one state at a time, supporting our selection of the ordering of states, and suggesting the suitability of a sequential morphology model. Transitions to higher states occurred under rising wave energy and were evenly spread among the possible higher states, with more substantial changes in morphology resulting from larger wave increases. This suggests that up-state, erosional transitions (based on offshore bar migration) are better described by an equilibrium model where response is better correlated with incident wave energy than with preceding morphological state. Time exposure images were also digitized to yield quantitative estimates of bar crest location as a function of longshore distance. Principal component analysis was used to decompose bar position into two-dimensional (linear) and three-dimensional (longshore variable) components. Cross-shore (linear) bar position ranges ±50 m about the 2-year mean (27 m standard deviation) and dominates bar variability (74.6%). Three-dimensional bar structure accounts for ~14% of the variance (12 m standard deviation). Changes in incident wave height precede cross-shore bar migration by less than 1 day. Changes in longshore variability are inversely correlated to changing wave conditions, with bar morphology becoming linear rapidly during storms (on time scales of less than 1 day). Evolution to significantly three-dimensional structure typically occurs over 5–7 days following peak wave events.

INTRODUCTION

The dynamics of nearshore beach topography have proved to be complex. Considering that bars are significant reservoirs of sand and modify the response of beaches to variable input wave conditions, the position and variability of these large-scale features has important implications for both long-term and short-term beach stability. Therefore, quantitative investigations of morphologic bar changes will yield valuable insight to processes controlling nearshore topography.

Descriptions of natural sand bar systems have been extensively reported in the literature, with forms ranging from two-dimensional linear longshore bars (with no longshore variability) to three-dimensional crescentic bars with coherent longshore periodicity. The first attempts to characterize the transition between bar forms were related to an annual cycle in wave energy and resulted in identification of "summer" and "winter" profiles with bars located farther offshore during higher-energy months. Later, *Sonu* [1973] noted that beach cycles involving crescentic bars could be a response to a series of storms, on much shorter time scales, and that bars tended to migrate shoreward under swell conditions. Many authors have also observed that erosional sequences were associated with the growth of waves, and accretional transitions with the subsidence of waves [e.g., *Sonu and James*, 1973]. However, the morphologic response to random storm events is still poorly understood.

Field studies have documented the behavior of topographical beach changes under the influence of variable fluid motions. Interpretations of data have followed two lines: development of models for equilibrium (static) bar formation which predict the form and scales that a bar would approach asymptotically under nonvarying incident wave conditions, and development of sequential morphologic state models which predict the sequence of bar shapes under variable incident wave conditions. The distinction between equilibrium and sequential models may also be defined operationally as whether the correlation with morphology is stronger with wave height or more dependant on its previous state, respectively.

A number of authors have devised conceptual, equilibrium models for linear bar formation through processes based on the plunging of incident waves [*Keulegan*, 1948; *Shepard*, 1950; *Miller*, 1976], the shoaling and breaking regions of incident waves [*Greenwood and Davidson-Arnott*, 1979], and the antinode or nodal location of waves standing in the cross-shore such as reflected incident waves [*Carter et al.*, 1973; *Lau and Travis*, 1973; *Short*, 1975; *Bowen*, 1980] or progressive edge waves [*Bowen*, 1980]. These standing wave models have an advantage in that they predict the cross-shore length scale of the bar from the standing wave period using

$$x = \frac{g\beta\chi}{\sigma^2} \tag{1}$$

where g is gravitational acceleration, β is beach slope, χ is a constant, and σ is the radian frequency of the standing wave ($\sigma = 2\pi f$).

Other equilibrium models have also been proposed for the generation of three-dimensional or crescentic bar forms. *Bowen and Inman* [1971] first showed that crescentic bars could be formed by the drift velocities associated with standing edge waves. This work was later extended by *Holman and Bowen* [1982] to the formation of oblique and other more complicated bar systems. These models also predict cross-shore length scales,

Paper number 90JC00272.
0148-0227/90/90JC-00272$05.00

and further predict the longshore length scales associated with periodic three-dimensional bars. Using the edge wave dispersion relation for a plane beach [*Ursell*, 1952], the crescentic bar wavelength is

$$L = \frac{gT_e^2}{4\pi} \sin(2n+1)\beta \quad (2)$$

where T_e is the period of the edge wave and n is the edge wave mode number. All equilibrium models assume that the bar response is essentially instantaneous.

Sequential models have arisen empirically from studies of beach topography that have similar but distinct origins: those that are based on single cross-shore profiles and those which incorporate longshore variability in the beach topography. In the first, field studies were restricted to single profiles periodically surveyed over varying lengths of time [e.g., *Sonu and van Beek*, 1971; *Sonu and James*, 1973; *Aubrey*, 1979; *Aubrey et al.*, 1980; *Aubrey and Ross*, 1985; *Birkemeier*, 1985]. These studies focused on the cyclic behavior associated with cross-shore sediment transport, most notably characterized by the seasonal cycle in accretion and erosion. Longshore variability in on-offshore sediment transport was not addressed.

In the second type of sequential model, considerable research has been directed toward understanding and predicting the shape and position of nearshore bars in terms of a set of morphologic states which qualitatively predict the sequence of beach morphology. Ordered sets of bar types, or classification schemes, have been presented (with varying degrees of success) that include the range of possible morphologies observed on natural beaches [*Greenwood and Davidson-Arnott*, 1979; *Chappell and Eliot*, 1979; *Short*, 1979; *Wright et al.*, 1979; *Goldsmith et al.*, 1982; *Wright and Short*, 1983; *Wright and Short*, 1984; *Sunamura*, 1988]. Some of these investigators have correlated beach states with wave height and wave power, or various surf similarity parameters, yielding a qualitative understanding of the conditions most closely associated with each state.

Wright and Short [1984] present the most highly evolved classification scheme, summarized on the left side of Figure 1. They specify six beach states ranging from completely dissipative to completely reflective. Beach classification is based on a series of characteristics, the most representative of which is bar morphology. They use a morphodynamic data base spanning more than 6 years and consisting of visual surf zone observations from a number of environmentally different beaches. *Wright et al.* [1985] and *Wright et al.* [1986] use this model to form empirical correlations between beach state and various parameters, most notably a weighted, running mean of the dimensionless fall velocity parameter $\Omega = H/(wT)$, where H and T are wave height and period and w is the sediment fall velocity at the bar crest [*Gourlay*, 1968; *Dean*, 1973]. Though the scheme appears to encompass (reasonably well) the entire range of possible beach states, not all of the classification definitions are unique. The most notable ambiguities are related to the longshore structure of the bar.

Most previous long-term studies, like *Wright and Short*'s [1984] study, were based primarily on visual observations in which three-dimensional bar characteristics were inferred from patterns of incident wave breaking. This method is not constrained by longshore coverage and has provided valuable insight. However, the quantitative information on bar position and length scales has been limited. Only very large scale structures can be identified; more subtle features of the bar are not resolvable with confidence. As a result, little quantifiable evidence has been presented regarding the stability of bars and time scales associated with large-scale morphologic change [e.g., *Goldsmith et al.*, 1982]. In recent field studies (e.g., the DUCK85 and SUPERDUCK experiments) intensive daily three-dimensional surveys provided valuable quantitative information about bar evolution but required enormous logistic effort [*Sallenger et al.*, 1985; *Howd and Birkemeier*, 1987*a*, 1987*b*; *Mason et al.*, 1987; *Crowson et al.*, 1988; *Birkemeier et al.*, 1989].

The aim of the present study was to quantify the temporal and spatial variability of sand bar morphology. Of particular interest is the evolution of three-dimensional morphology in relation to high-energy storm events. Morphologic data were collected over a 2 year period using a time exposure video technique [*Lippmann and Holman*, 1989]. The analyses presented follow two distinct lines. First, observed morphologies (bar samples) are classified into an eight-state model based on four classification criteria. Second, time series of bar crest position are decomposed into two-dimensional (linear) and three-dimensional components using empirical orthogonal functions. For both analyses, comparisons are made with incident wave parameters, and response time scales are estimated.

METHOD OF SAMPLING MORPHOLOGY

The method for sampling bar morphology must satisfy three criteria. First, the shape of the bar must be easily identified so that classification distinctions can be made. Second, the position of the bar crest must be accurately measured over a range of longshore distances. Third, sampling must be possible across the entire range of conditions.

In this study, we exploit a recently developed remote sensing technique—time-averaged imaging of incident wave breaking—which rapidly estimates the location of the bar crest over large alongshore distances. The technique is not constrained by high-energy storms and therefore may be employed when scientific interest is greatest and more traditional sampling methods must be abandoned; however, the technique fails under very low waves. The technique is presented fully by *Lippmann and Holman* [1989] (henceforth LH89) and is only summarized here.

The technique is based on the preferential breaking of incident waves over the shallows of a bar, similar to past visual observational methods. The sharp contrast in light intensity between breaking and nonbreaking regions may be imaged photographically; however, instead of using an instantaneous "snapshot," we employ a long time exposure (typically 10 minutes), thereby averaging out fluctuations due to incident wave modulations and giving a statistically stable image of the incident wave breaking pattern (Figures 2*a*–2*h*). Peaks in cross-shore intensity indicate the presence of a sand bar, while the shoreline is indicated by an intensity maximum at the water's edge. Clearly, the technique is valid only if waves are breaking over the bar.

Time exposure images are created from video recordings of the surf zone by digitally averaging individual frames over a 10-minute period using an image-processing system. Pixel (picture elements) locations may be transformed into corresponding ground coordinates using photogrammetric relationships [LH89]. Shore normal transects of light intensity may then be digitized, in which intensity maxima occur at the shoreline (a result of the shore break) and in the vicinity of the bar crest.

Calibration studies have shown that the location of the shoreline and longshore variability in bar form are both accurately measured using this technique (denoted conventional

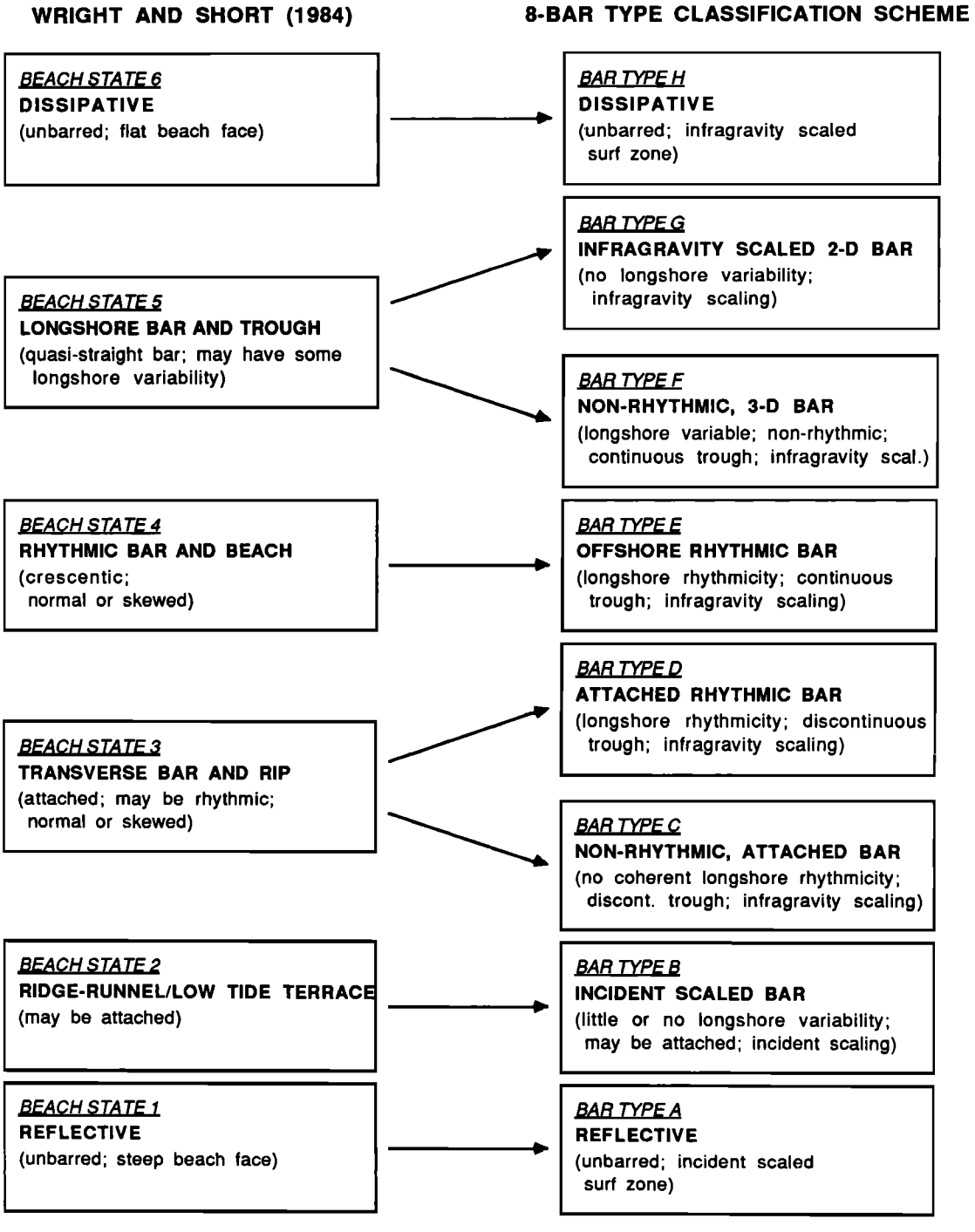

Fig. 1. Classification scheme of *Wright and Short* [1984], shown on the left-hand side. Our classification scheme is presented on the right-hand side. Comparisons between the two models are indicated with arrows between similar morphologic bar states.

time exposures in this text) [LH89]. However, because of an accumulation of persistent foam near the shoreward edge of the bar crest, cross-shore estimates of bar crest locations may be displaced landward during high energy conditions. To remove this bias, an image differencing technique is employed. Persistent foam, not associated with actively breaking waves and bores, is removed by subtracting successive video frames and averaging the difference images. The result, called a differencing time exposure, proves better for locating the actual position and longshore variability of the bar crest. The differencing procedure, although fairly robust, requires good video quality and incorporates two free parameters: the time interval between successive frames and a threshold (intensity) noise level. Best results were found when these values were set at 1 second and ~6% of the maximum range of intensity, respectively.

Experimental errors result from two sources. The first is simply related to the photographic resolution of the image. For this study, at worst resolution, errors were always less than 2.0% of the

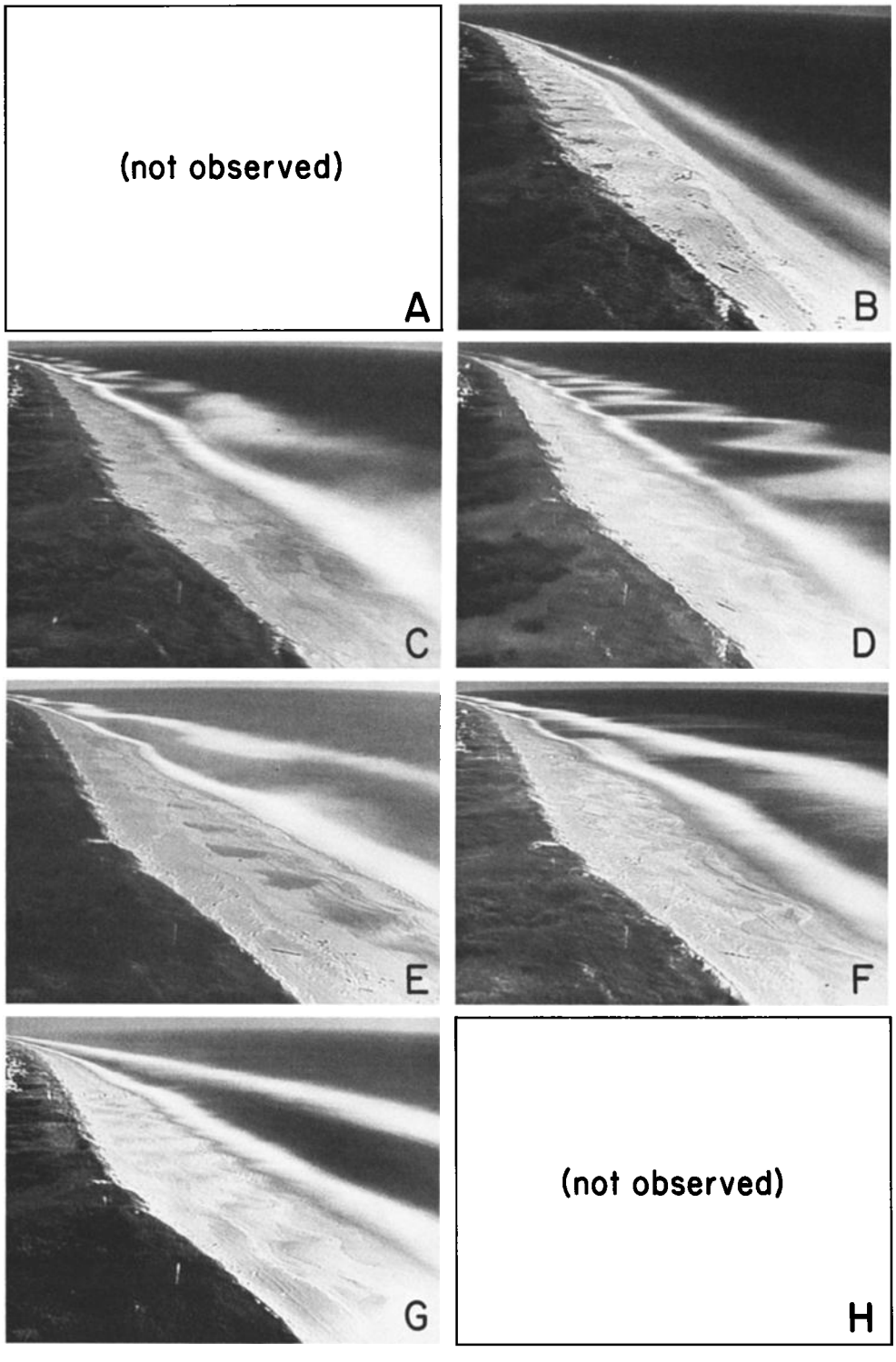

Fig. 2. Example time exposures which best represent the observed morphologies at the field site. (*a*) Bar Type A; not observed. (*b*) Bar Type B; August 9, 1987. (*c*) Bar Type C; January 10, 1988. (*d*) Bar Type D; October 17, 1987. (*e*) Bar Type E; January 25, 1987. (*e*) Bar Type F; March 6, 1987. (*g*) Bar Type G; December 25, 1986. (h) Bar Type H; not observed.

distance to the camera (less than ±1 m in the cross-shore and ±2.5 m in the longshore). A greater error arises from the location of maximum wave dissipation, in which the estimated bar crest positions are weighted offshore from the true bar crest location by a small amount that varies with the tide. Percentage errors are generally on the order of less than 5–10% of the cross-shore distance to the crest (with theoretical worst case errors of less than 35% [LH89]). For this study the average error is estimated to be less than 15 m seaward of the crest and does show a tidal dependence.

METHODS OF CHARACTERIZING MORPHOLOGY

Sequential Classification Scheme

We choose to define bar types on the basis of four characteristics of their morphology:

1. Existence or absence of a bar. Existence implies the realization of a discernable trough region where little or no incident wave breaking occurs (imaged as a darker region between the lighter breaking pattern over the bar and the shore break).

2. Dominant bar scaling: incident versus infragravity. Bar scaling (equations (1) and (2)) is considered incident if the dominant cross-shore and longshore length scales (if applicable) of the bar are roughly equal to the local incident wavelength scales (typically on the order of 10 m). Bar scaling is considered infragravity if the dominant length scales are much longer (of order 10^2–10^3 m). In the absence of an obvious bar, the width of the surf zone is used as a proxy measure to define representative length scales.

3. Longshore variability: linear (no variability), rhythmic, or nonrhythmic. Longshore rhythmicity is indicative of crescentic bars, welded bars, or regularly spaced rip channels.

4. Trough: continuous or discontinuous. The trough is considered discontinuous when the bar is attached to the shoreline, indicated by regions of continuous breaking from the bar to the shoreline.

This set of classification criteria form a system of binary (one is actually tertiary) decisions leading to unique bar definitions, illustrated by a flow chart (Figure 3) and look-up table (Table 1). These criteria can be related to processes thought to be important in controlling nearshore morphology, particularly bar scaling (equations (1) and (2)) and longshore variability. Use of the scheme requires a number of subjective decisions. Rhythmicity, for instance, does not require perfect periodicity but implies that the structure is more regular than unorganized. Similarly, trough continuity is generally assumed unless the bar is obviously attached at numerous locations alongshore. Note that in this model we do not attempt to distinguish between incident scaled bars with varying degrees of longshore rhythmicity (since they were never observed). Also, criteria are used to describe characteristics of only the inner bar with no regard to the possible presence of multiple bars. Clearly, the last two criteria are not applicable for fully dissipative and reflective beaches.

The resulting model encompasses eight morphologically different bar types (shown on the right-hand side of Figure 1). Bar types at the top of the scheme will be referred to as higher bar types; those at the bottom are considered lower bar types. This model is easily compared with *Wright and Short*'s [1984] six-state model (shown on the left-hand side of Figure 1). Our definitions break up two states in Wright and Short's model. Their Longshore Bar and Trough, is divided into two bar types, one representing linear bars with no longshore variability (Bar Type G) and the other representing bars with nonrhythmic longshore variability (Bar Type F). Their Transverse Bar and Rip state is also divided into two bar types, each attached to the shoreline and with longshore variability distinguished by the presence (Bar Type D) or absence (Bar Type C) of dominant periodicity. The other bar types remain essentially the same.

This scheme has several distinct advantages. For single-barred systems (or by considering only the innermost bar for multibarred cases), the set is complete and unique. It spans the complete set of all possible large-scale bar states, ranging from fully dissipative to fully reflective. Furthermore, each state is defined by discrete morphologic descriptions. Finally, the distinguishing criteria (particularly scaling and longshore variability) can be directly related to the testing of bar generation models, for example, the scale of infragravity models or the existence of standing wave patterns.

Example time exposure images which best represent the observed morphologies (Bar Types B–G) are shown in Figure

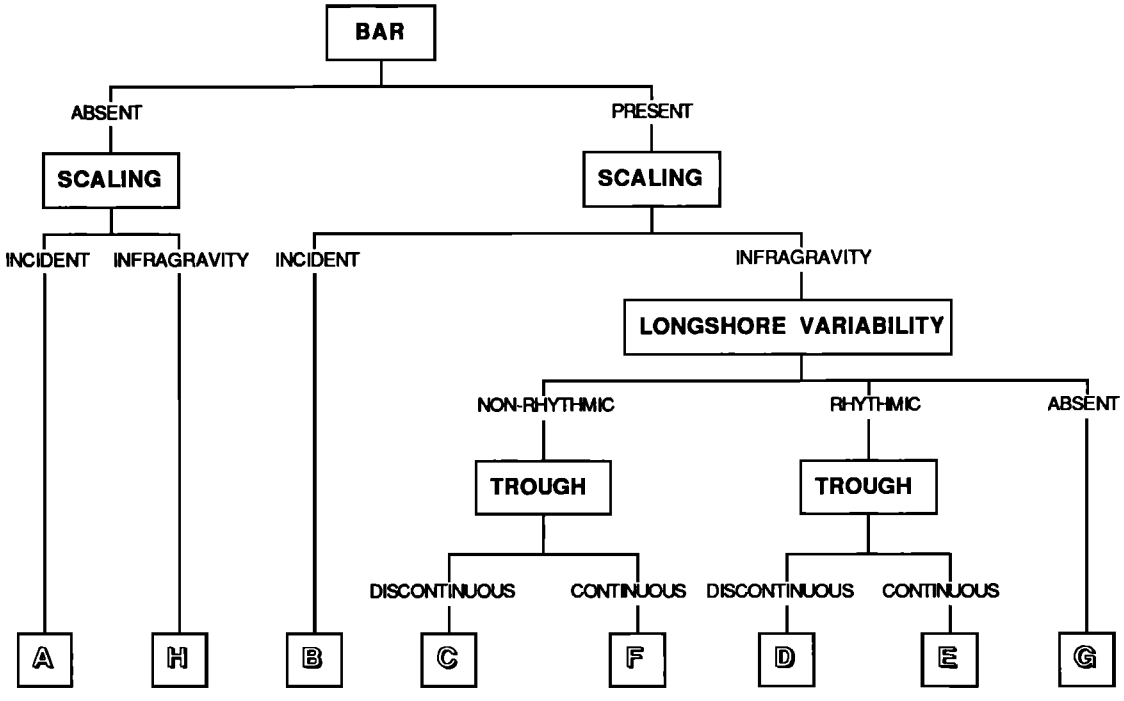

Fig. 3. Classification criteria arranged in a workable flow chart. Morphologic classifications are based on one tertiary and three binary decisions. Each individual morphologic bar type (from the right-hand side of Figure 1) is uniquely defined in this manner.

TABLE 1. Classification Criteria Used to Describe Bar Morphology

Bar	Scaling	Longshore Variability	Trough	Bar Type
0	1	N/A	N/A	H
1	1	0	1	G
1	1	1	1	F
1	1	2	1	E
1	1	2	0	D
1	1	1	0	C
1	0	0,1,2	0,1	B
0	0	N/A	N/A	A
(absent, 0; present, 1)	(incident, 0; infragr., 1)	(absent, 0; non-rhyth., 1; rhythmic, 2)	(discont., 0; continuous, 1)	

N/A, not applicable. Each corresponding bar type uniquely defined in this manner is shown in the last column.

2*a*–2*h*. The two extreme morphologic bar types (Bar Types A and H), though sometimes observed at other field sites, were never identified at the Duck field site and so no examples are presented. These examples are made from conventional 10-minute time exposures which yield the best view of the bar. When using these images to classify bars, one must keep in mind the possibility of residual foam accumulation causing a landward bias in the position of the bar, which might alter decisions involving cross-shore scaling and trough continuity (discussed further by LH89).

The classification procedure was tested by nine individuals (with varying degrees of familiarity with nearshore processes) using a subset of 60 selected images covering the range of observed bar types. Figure 4 shows the variability of classifying each morphologic bar sample into the different classes. Tabulations for all individuals together showed that an average of 75% (±8%) of the classified samples agreed with the consensus bar type. Nonrhythmic bars were the most difficult to classify, with the most troublesome classification criteria involving the continuity of the trough and the determination of longshore rhythmicity. In general, our sampling method and classification scheme was found to be fairly robust in uniquely identifying each bar sample.

Longshore Structure of Bar Crest Position

The second method of describing sand bar morphology was to analyze the behavior of the bar crest position, $x_c'(y,t)$. The data used in this analysis are in the form of digitized x_c' locations (from daily differencing time exposure images) at numerous longshore locations. This signal can be objectively separated into two components, one representing the two-dimensional (linear) movement and the other representing the three-dimensional (longshore variable) behavior.

We accomplish this by restructuring the data using standard principal component, or EOF, analysis [*Priesendorfer et al.*, 1981]. The mean corrected data, $x_c(y,t)$, are decomposed into orthogonal spatial factors, $e_j(y)$, and corresponding amplitude time series, $a_j(t)$, such that

$$x_c(y,t) \approx \sum_{j=1}^{p} a_j(t)e_j(y) = A(t)e_1(y) + \sum_{j=2}^{p} a_j(t)e_j(y) \quad (3)$$

where t is time and y is longshore position. A linear factor, $e_1(y)$, represents the linear deviation of the sample mean bar position (over the length of the array), $\bar{x}_c(t)$, from the data mean, $\tilde{x}_c$

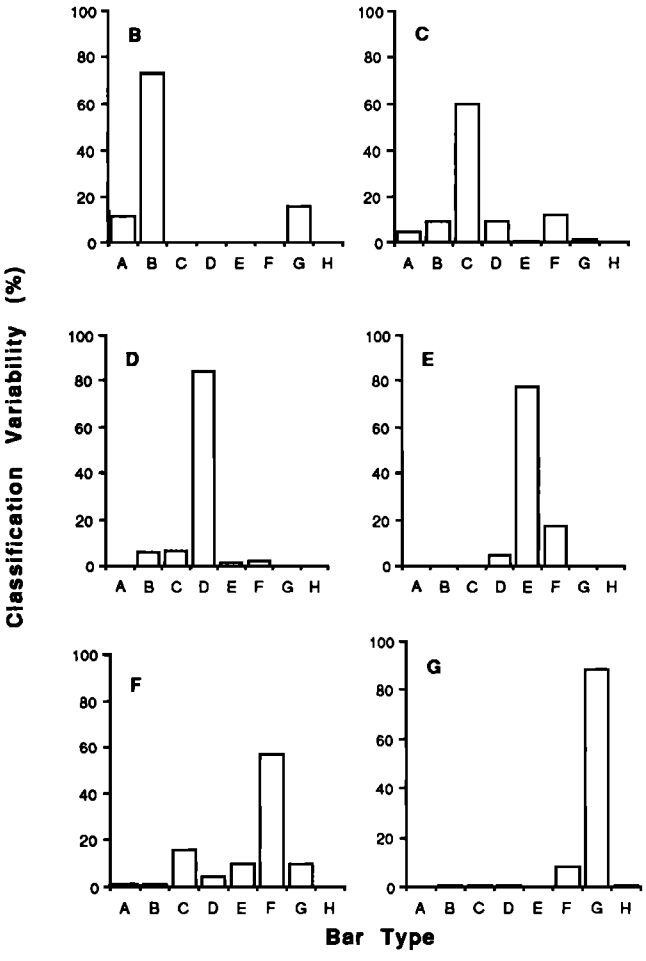

Fig. 4. Results from morphological classification tests showing the tendency to classify bar types in states other than the consensus state. The highest percentage of classified bar type defines the consensus bar type, indicated by the bold letters in the upper left corner of each graph.

(described later), and thus the corresponding amplitude time series, $a_1(t)$ (henceforth referred to as $A(t)$), represents a quantified measure of the mean cross-shore bar movement. (Note that a linear factor need not necessarily contain the highest percentage of variance.) The remaining spatial factors are representative of three-dimensional bar structure and have a collective variance, $V(t)$, given by

$$V(t) = \sum_{y} \left(\sum_{j=2}^{p} a_j(t)e_j(y) \right)^2 \quad (4)$$

that quantifies the degree of longshore variability of the bar crest. Note that the series has been truncated at "p" significant factors to reduce the effect of noise in the analysis.

Field Techniques and Data Collection

The data were collected as part of a long-term monitoring program at the Army Corps of Engineers CERC Field Research Facility (FRF) on the Outer Banks of North Carolina near the village of Duck [*Birkemeier et al.*, 1985]. The area of interest ranges from dune crest to 200 m offshore, begins approximately 180 m north of the FRF research pier, and extends 660 m alongshore to the north. *Miller et al.* [1983] showed that this region is outside the area affected by the pier pilings.

The beach at Duck is characterized by a persistent, very dynamic, inner bar located approximately 30–120 m offshore, and a more stable outer (storm) bar approximately 300–400 m offshore. The beach foreshore is predominantly steep, $\tan\beta \approx 0.08$ (1:12.5), and the shoreline is very stable, consisting of a mixture of medium quartz sand (mean grain size ≈ 1 mm) and carbonate shell debris (up to 20%). Offshore, the bottom slope approaches $\tan\beta \approx 0.0061$ (1:164) near the 8-m depth contour, and the median grain size decreases to ~0.1 mm. The wave climate is variable throughout the year, with higher wave conditions dominated by extratropical nor'easters during the fall, winter, and early spring months. The summer months are characterized by lower-amplitude, long-period swell from the southeast, with occasional tropical hurricanes during the late summer and fall. The spring tide range at Duck is ~1.5 m. A more complete description of the beach conditions is given by *Birkemeier et al.* [1989].

Video data were collected using a black-and-white television camera mounted on top of a 40-m-high tower erected on the dune crest 63 m north of the pier (Figure 5). Daily video records of 15 minute length were acquired from October 7, 1986, through October 1, 1988. Conventional and difference time exposure images of 10-minute length were created digitally using an image processing system. Each conventional time exposure was classified several times according to the previously presented scheme. In addition, 34 shore normal intensity profiles spaced 20 m apart alongshore were digitized from the images and analyzed to give estimates of shoreline and bar crest position.

Gaps exist in the time series of bar morphology for three reasons. First, occasionally the waves were too small to break on the inner bar; second, adverse environmental conditions such as snow and fog prevented the use of photographic imagery; and third, recording occasionally failed (including a 3-week period from April 13 to May 4, 1987). Marginal records were not included for the morphological analysis if image quality was too poor to allow a clear view of the bar. Differencing time exposure records were also eliminated from the EOF analysis if at least 50% of the 34 longshore estimates of x_c were missing (or undetectable). Occasional missing estimates were interpolated in the following manner:

$$x_c(y_i,t_j) = x_c(y_i,t_{j-1}) + (\bar{x}_c(t_j) - \bar{x}_c(t_{j-1})) \quad (5)$$

where the overbar denotes the longshore mean. That is, the interpolated value at a location is just the previous value at that location plus the change in the mean bar position over the time between adjacent samples. Inspection showed the method to work reasonably well with minimal introduction of systematic errors. A total of 523 days (72.2% of the total record) were used for the classification analysis, and 476 days (65.7%) were used in the EOF analysis.

Ancillary measures used in this study include 20-minute averages at 6 hour intervals of significant wave height, H_s, and peak incident wave period, T, collected by the FRF staff using a waverider buoy located 6 km offshore. Missing data values were augmented using a Baylor wave gage located at the end of the pier.

RESULTS

Morphologic Stability

From the daily estimates of morphology, the probability of occurrence of each bar type, P_i, was found as the number of days for which state "i" was observed, divided by the total number of sample days. Also, the number of transitions to a particular state, N_i, and the residence time, τ_i, within each state were tabulated. These measures are related in the following way:

$$P_i = \frac{N_i \langle \tau_i \rangle}{\sum_k N_k \langle \tau_k \rangle} \quad (6)$$

For the transition calculations, gaps in the data of less than 5 days (occurring on five occasions) were ignored. Results are shown in

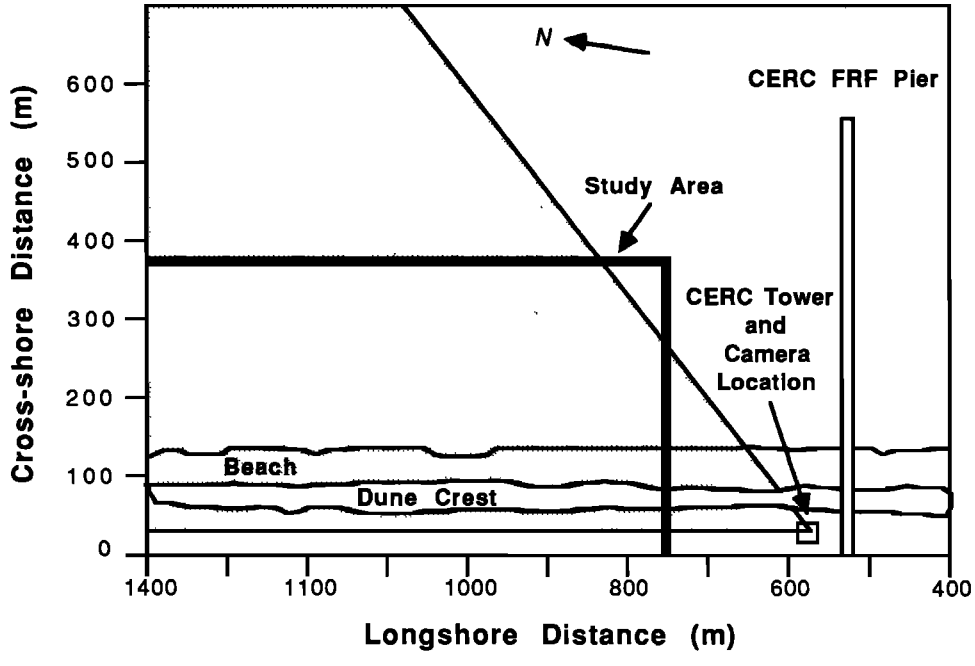

Fig. 5. Map of the field site for the 2-year data record. The position of the camera in relation to the FRF pier and the study area is indicated. Longshore and cross-shore distances are relative to the FRF coordinate system. The stippled area indicates the ground coverage in the field of view of the camera.

Table 2 and Figure 6. The probability of occurrence parameter, P_i, is similar to *Short*'s [1979] beach state curve and *Wright and Short*'s [1984] "percent occurrence of beach states."

Residence times, demonstrated by their means, $\langle\tau_i\rangle$, and standard deviations, s (Table 2 and Figure 6), are a measure of bar persistence and, in some cases (such as for linear bars) when used in conjunction with antecedent wave conditions, may be interpreted as a measure of bar stability. Figure 6 shows high bar states are short-lived, with lower bar types remaining for progressively longer durations (with the exception of Bar Type C). However, there is also a large amount of variability in τ_i, indicated by the high standard deviations in comparison to the means. Further analysis (later in this section) shows that most upward transitions (based on the scheme presented in Figure 1) occurred very rapidly, whereas transitions down were more often gradual, especially for the lowest bar types.

TABLE 2. Percent observations, P_i, number of transitions N_i, and average residence times, $\langle\tau_i\rangle$, for each bar type

Bar Type	P_i (%)	N_i	$\langle\tau_i\rangle$ (days)
H	-	-	-
G	6.7	19	2.1
F	13.8	29	2.9
E	24.0	30	4.7
D	43.6	22	11.1
C	3.3	6	3.2
B	8.6	3	18.0
A	-	-	-

The most common bars observed were attached rhythmic bars, Bar Type D (P_D = 43.6%); higher bar types (E–G) were seen on progressively fewer occasions. Even though Bar Types E and F occurred more often (N_E = 30; N_F = 29) than Bar Type D (N_D = 22), they were observed less often (P_E = 24%; P_F = 13.8%), a consequence of their shorter residence times. The lower bar types, B and C, were rare (N_B = 3; N_C = 6). The linear bar, Type G, though relatively uncommon (P_G = 6.7%), did occur on many different occasions as morphology changed (N_G = 19). Incident scaled features were never observed in bars with longshore variability and only occurred in the form of quasi-straight ridge-and-runnel or low-tide terrace bars, Bar Type B. The differences in N_i and P_i are attributed to the relative stability of the individual morphologic forms.

The sequence of transition between the various bar types was also investigated (Table 3). The ij^{th} element in the table represents the percentage of transition from state j to state i. Transitions to lower bar types (below the diagonal) usually occur sequentially, with 86.6% of downward transitions being single step. On the other hand, transitions to higher bar types (above the diagonal) are more evenly distributed among higher states (only 49.5% being single step). All bar types are observed to jump (i.e., move rapidly with respect to our minimum sampling interval of 1 day), at least on some occasions, to the highest state, Bar Type G. Thus, for up-state transitions the final state is relatively independent of its initial state, but for down-state transitions the bar depends more heavily on its previous configuration. However, this result may be a natural consequence of the time scale response of the bar to the wave forcing and with resolution a function of our sampling interval.

The average wave conditions corresponding to the occurrence of each state were also found. Mean statistics were calculated for

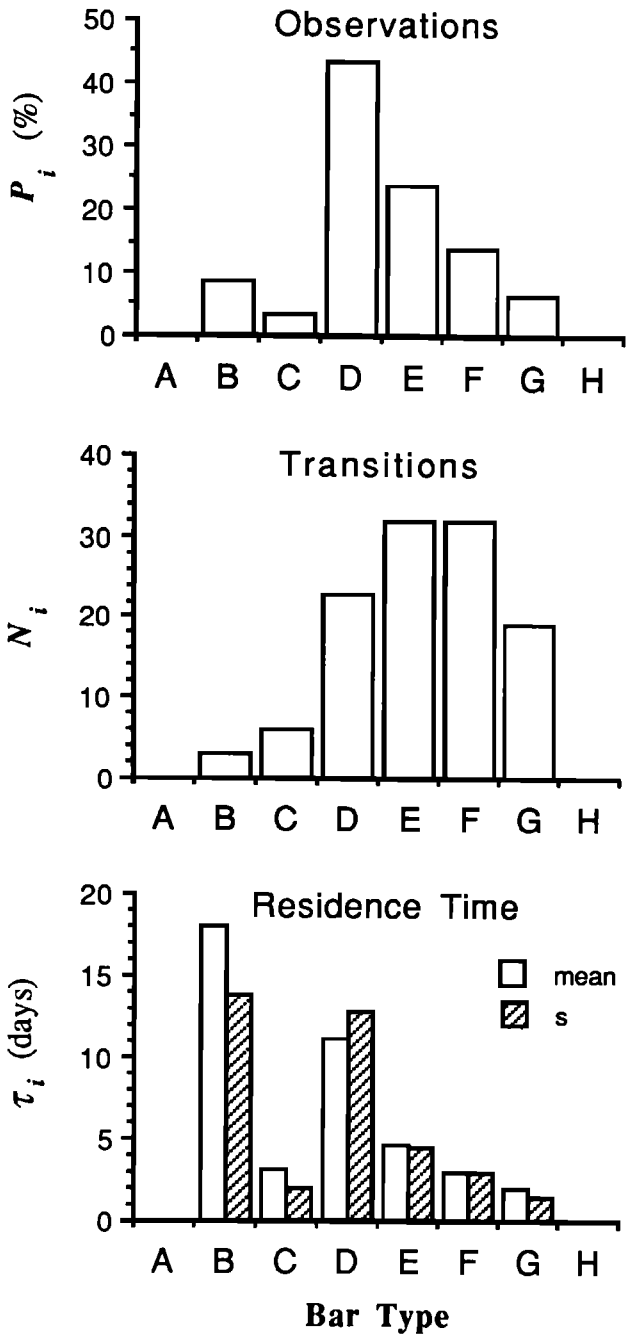

Fig. 6. Histograms of probability of bar occurrence (%), P_i (upper panel), total number of transitions, N_i, to each state (middle panel), and mean, τ_i, and standard deviations, s, residence times for each state (lower panel).

significant wave height, $\bar{H}_s$, incident wave power, $\bar{P}_0 = \rho g^2 H_s^2 T^2/32\pi$ (proposed as important in parameterizing morphologic change by *Short* [1979]), offshore wave steepness, $\overline{H_0/L_0}$ (the wave part of the Iribarren surf similarity number, $\xi_0 = \beta/(H_0/L_0)^{0.5}$, proposed by *Hunt* [1959]), and finally $\overline{H_s/T}$ (the wave part of the dimensionless fall velocity parameter mentioned earlier). When compared to our morphologic bar types, we find that all these parameters behave in a similar manner (Figure 7), which is largely a result of the variables themselves being highly correlated.

Linear bars are associated with the highest waves ($\bar{H}_s$ = 1.75 m), predominating at the peak of high-energy storm events. Bars

TABLE 3. Percent Transitions Between Morphologic Bar Types

	From							
To	A	B	C	D	E	F	G	H
H	·	·	·	·	·	·	·	+
G	·	33(1)	17(1)	26(6)	23(7)	14(4)	+	·
F	·	·	33(2)	23(5)	23(7)	+	84(16)	·
E	·	·	·	23(5)	+	83(24)	5(1)	·
D	·	67(2)	50(3)	+	47(14)	·	11(2)	·
C	·	·	+	14(3)	7(2)	3(1)	·	·
B	·	+	·	14(3)	·	·	·	·
A	+	·	·	·	·	·	·	·
N_t	0	3	6	22	30	29	19	0

The actual numbers of transitions are shown in parentheses. Initial states are along the top, and resulting states are listed on the left. The total number of transitions to each state, N_t, are shown at the bottom of each column. Note that transitions are recorded based on the resolution of our sampling interval (1 day).

TABLE 4. Mean Significant Wave Height, $\bar{H}_s$, (bold) and Mean Change in $\overline{\Delta H_s}$ for Each Transition

	From							
To	A	B	C	D	E	F	G	H
H	·	·	·	·	·	·	·	+
G	·	**1.69*** +1.11	**2.07*** +1.50	**1.95** +0.98	**1.98** +1.10	**1.02** +0.13	+	·
F	·	·	**1.90*** +0.92	**1.45** +0.41	**1.52** +0.76	+	**1.39** -0.27	·
E	·	·	·	**1.03** -0.11	+	**1.02** -0.37	**0.82*** -1.22	·
D	·	**1.09*** +0.51	**1.18** +0.25	+	**1.15** +0.17	·	**1.62*** -0.79	·
C	·	·	+	**1.01** +0.23	**2.66*** +0.54	**0.71*** +0.02	·	·
B	·	+	·	**0.52** +0.03	·	·	·	·
A	+	·	·	·	·	·	·	·

Initial states are along the top, and resulting states are listed on the left. Erosion occuring from bottom to top in the table and accretion from top to bottom.

*Computed from less than three transitions.

with longshore variability are associated with lower wave energy ($\bar{H}_s$ = 0.9–1.27 m), whereas quasi-linear incident scaled bars occur under the lowest mean wave conditions ($\bar{H}_s$ = 0.58 m). In general, higher bar types are associated with higher values of all wave parameters, similar to observations reported by previous authors [e.g., *Short*, 1979; *Goldsmith et al.*, 1982; *Wright et al.*, 1985]. The middle bar types, C, D, and E, occur under similar, intermediate wave conditions. Analyses to follow indicate that no single parameter shows superiority over any other for this particular field site; therefore, for simplicity, we will focus further discussion on wave height dependance.

Relationships between wave parameters and changes in morphology are also illustrated with transition tables, similar to previous work by *Wright and Short* [1984]. The average wave parameters associated with each transition were calculated at the first occurrence of a new bar type. The changes in wave parameters were calculated as the first occurrence value minus the mean value for the preceding state prior to the transition. Table 4 shows $\bar{H}_S$ and $\overline{\Delta H_s}$ for the transitions. Down transitions are generally associated with lower $\bar{H}_s$, and since lower state bars are generally closer to the shoreline, are representative of "accretional" sequences. Up transitions to higher bar types are associated with larger waves and increasing wave energy (positive $\overline{\Delta H_s}$), indicative of "erosional" sequences, with jumps in morphology (with respect to our sampling interval) associated with higher waves (average $\bar{H}_s \approx 2$ m) and larger increases ($\overline{\Delta H_s} \approx +1$ m).

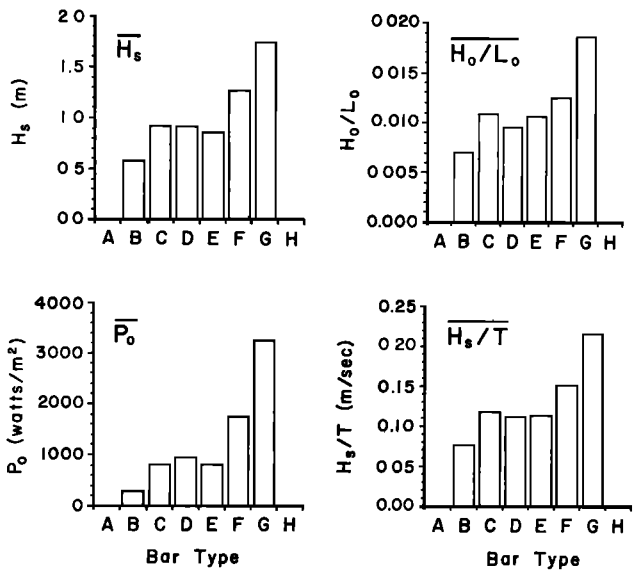

Fig. 7. Histograms of $\bar{H}_s$, $\bar{P}_0$, $\overline{H_0/L_0}$, and $\overline{H_s/T}$ for each bar type.

The linear bar, with low residence time ($\langle\tau_G\rangle \approx 2$ days), requires largest wave energy to maintain its form, with small declines in energy resulting in the development of longshore variability, with this bar type evolving almost exclusively (84%) into the next lowest state. The nonrhythmic states (Bar Types C and F) occur under similar wave conditions as the rhythmic states (Bar Types D and E), but are much less persistent ($\langle\tau_C\rangle \approx \langle\tau_F\rangle \approx 3$ days; $\langle\tau_D\rangle \approx 11$ days; $\langle\tau_E\rangle \approx 5$ days). Transitions between intermediate states appear to occur under small or minimal wave changes, illuminated by the commonly observed sequence in which unattached rhythmic bars (Bar Type E) migrate onshore under low wave conditions, maintaining longshore form, and eventually attaching to the shoreline (becoming Bar Type D, also noted previously by other authors, e.g., *Sonu* [1973]). However, we observe opposite transitions in which Type D bars transform into Type E bars (i.e., with the formation of a trough) under declining wave conditions ($\overline{\Delta H_s} = -0.11$m). In general, the transitional behavior of lowest bar types, usually occurring under relatively mild conditions, do not follow obvious trends with respect to changing wave energy.

Thus, the linear state, as well as nonrhythmic bars, may be considered relatively unstable, while rhythmic states seem much more stable with stability increasing as bars become attached to or, in general, move closer to the shoreline. Specific up-state transitions appear to be more dependant on $\bar{H}_s$ than do individual down-state transitions, which would seem to indicate that erosional sequences are more closely associated with equilibrium

conditions and that accretional transitions tend to be sequential. However, we cannot conclude that up-state transitions are not sequential, since the migration of the bar is faster than our sampling resolution (1 day). We do note that the time scale of response for up-state transitions (Table 3) is of the same scale as the wave changes (Figure 8), which is favorable for equilibrium modeling, whereas most response time scales for down-state transitions (with the exceptions of transitions from Bar Type G to Bar Type F and Bar Type F to Bar Type D) and are much longer than storm decay time, which is more favorable for sequential modeling.

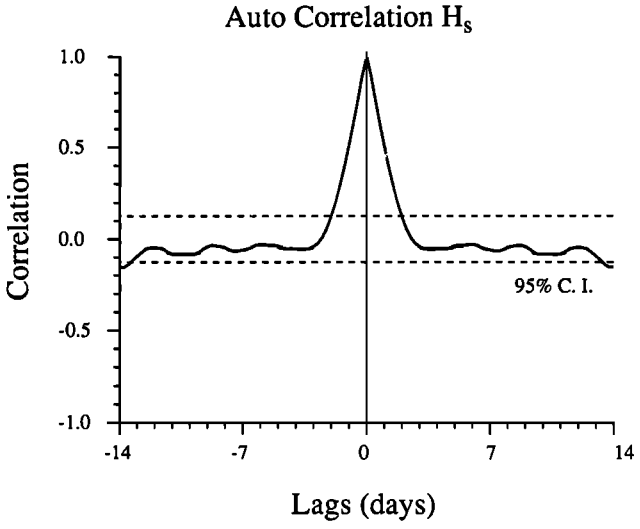

Fig. 8. Autocorrelation diagram for significant wave height, H_s, over the 2-year period for lags out to ±14 days. The 95% confidence intervals (dashed lines) were calculated using the long-lag artificial skill method [after *Davis*, 1976].

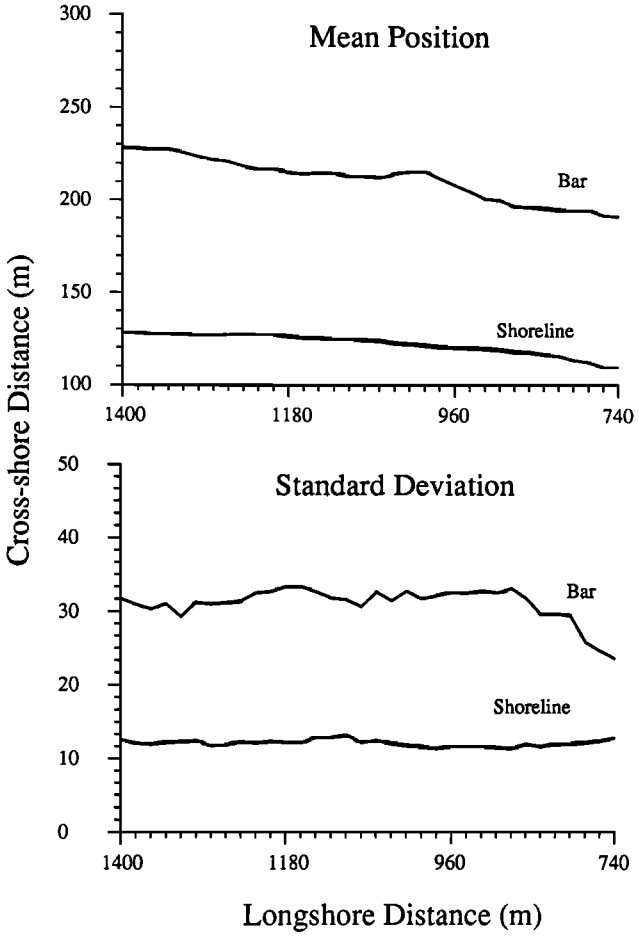

Fig. 9. Two-year mean shoreline and bar crest position for differencing time exposure data (upper panel) and the corresponding standard deviations alongshore (lower panel). The longshore and cross-shore distances are relative to the FRF coordinate system shown in Figure 5.

It should be noted that the terms "erosion" and "accretion" are not well-defined terms as we are using them. Although we recognize that erosion/accretion should be some measure of integrated cross-shore transport, these data are not available. We use the terms erosion and accretion to indicate times of onshore and offshore bar movement, respectively, consistent with previous work of *Wright and Short* [1984]. Since bars at Duck contain large volumes of sediment [*Birkemeier et al.*, 1989], our application of the terms seems reasonable for this field site.

Longshore Structure in Bar Crest Position

The mean shoreline, $\tilde{x}_s$, and mean bar crest position, $\tilde{x}_c$, for the 2 years of data are shown in Figure 9: $\tilde{x}_c$ is reasonably straight and parallel to $\tilde{x}_s$ and is located approximately 85 m offshore. A small (~10%) offshore increase in $\tilde{x}_c$ farther away from the camera is an artifact of the image differencing method [LH89]. This trend is removed with the mean and does not affect the following results. The standard deviation, s, is nearly constant alongshore indicating that $x_c(y,t)$ is homogeneous over the length of the sample area.

Figure 10 shows the decomposition of the mean-corrected bar crest data into the first five orthogonal EOFs ($e_j(y)$, equation (3)). Higher EOFs were considered to be insignificant, associated with sampling errors. EOF 1 is approximately linear, representing the mean cross-shore location of the bar; hence the first amplitude time series, $A(t)$, represents the time dependence of the two-dimensional morphologic component. The 2-year variability in bar position is dominated by cross-shore bar migration (74.6% variance associated with EOF 1), with a range of mean on-offshore bar movement of ±50 m about $\tilde{x}_c$ (s = 27 m).

The $A(t)$ time series reveals a predominant long-period signal representative of the well-known seasonal cycle in on-offshore sediment movement. There is also variability on a much shorter time scale. Though the range associated with this cycle (s = 19 m) is less than the annual cycle, its variability characterizes the short-term changes in bar position.

The next four EOFs represent longshore variability in bar crest position. These factors appear somewhat sinusoidal, a result of orthogonality constraints required in the analysis. Therefore, no attempt is made to correlate dominant wavelengths with length scales of observed rhythmic bars. Instead, we sum the factors and then calculate the longshore variance associated with each sample (equation (4)). The resulting variance time series, $V(t)$, represents the evolution of longshore variability associated with the three-dimensional component in bar position (although it does not distinguish rhythmic from nonrhythmic structure). The total percent variance associated with $V(t)$ is ~14% (s = 12 m), one-fifth the variance of the linear (two-dimensional) factor.

Cross-correlations between $A(t)$ and H_s for lags out to ±14 days are shown in Figure 11*a*. The high positive correlation at zero lag (r = 0.58, 95% significant level) indicates that the on-offshore

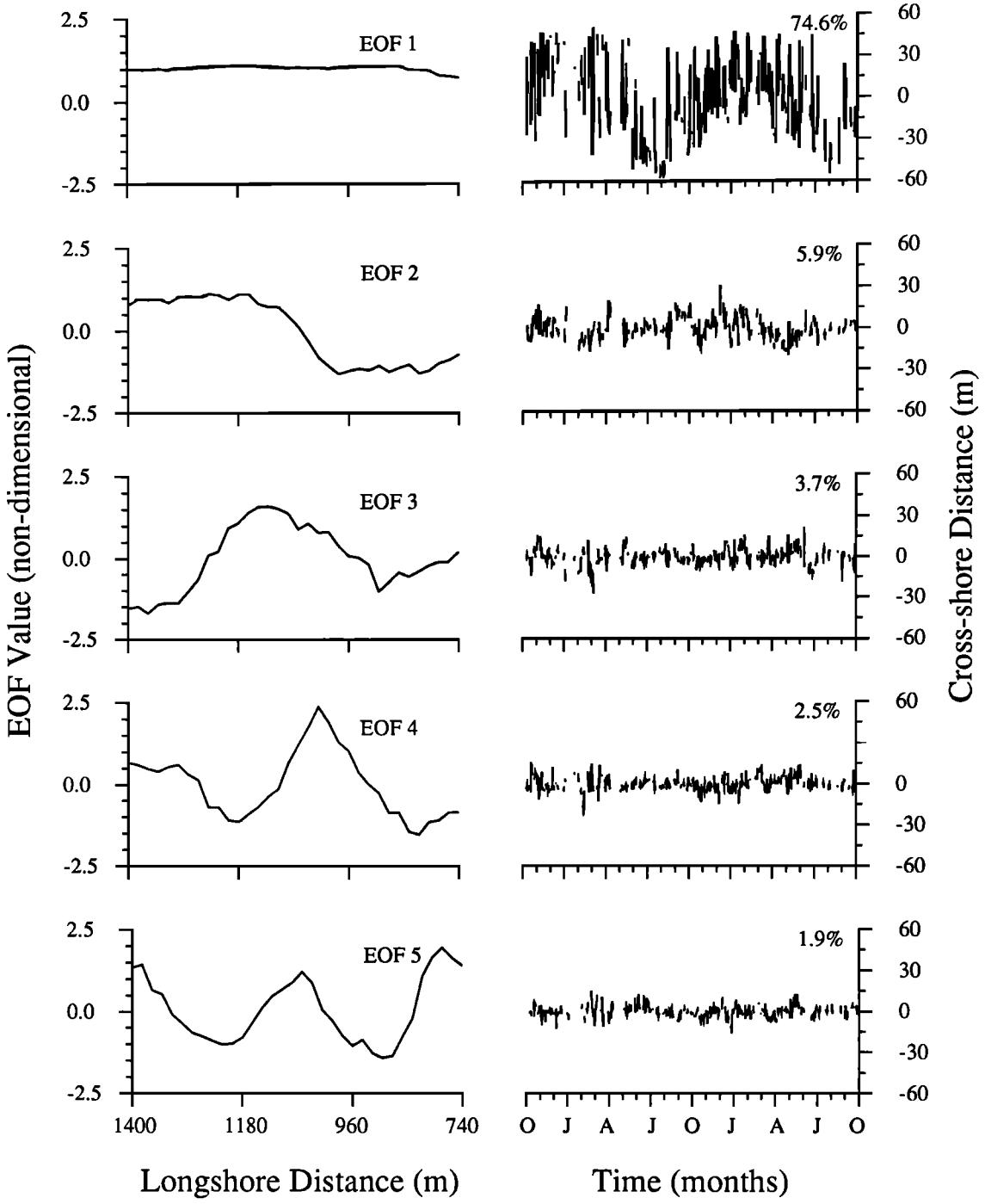

Fig. 10. The first five EOFs from the decomposition of the differencing bar crest data. Spatial factors are shown on the left side, where the longshore distance is relative to the FRF coordinate system and the EOF values are nondimensional. Corresponding amplitude time series are shown on the right side, along with relative variance contributions. The time scale (along the bottom) is in months, and the cross-shore distances are in meters and are relative to the 2-year mean (Figure 9).

movement of the mean bar position tends to be concurrent with decreases and increases in incident wave height. The consistently positive correlations at longer lags indicate that the long-period seasonal cycle is influencing the correlation results. Since our interest is primarily on much shorter time scales (that associated with random storms), the seasonal cycle is removed from the time series by block-detrending with 21-day means (a time scale much shorter than the annual signal and much longer than the average storm event).

Correlations using the detrended $A(t)$ is shown in Figure 11*b*. Again, high positive correlations centered about zero lag exist ($r = 0.62$). The decorrelation time scale indicates that previous wave events occurring more than about 2 days past do not significantly influence the position of the bar. Correlations with other parameters yielded similar results, but once again, best results (highest correlations) were found using H_s. All following analyses will be with time series that have the seasonal cycle removed by their 21-day means.

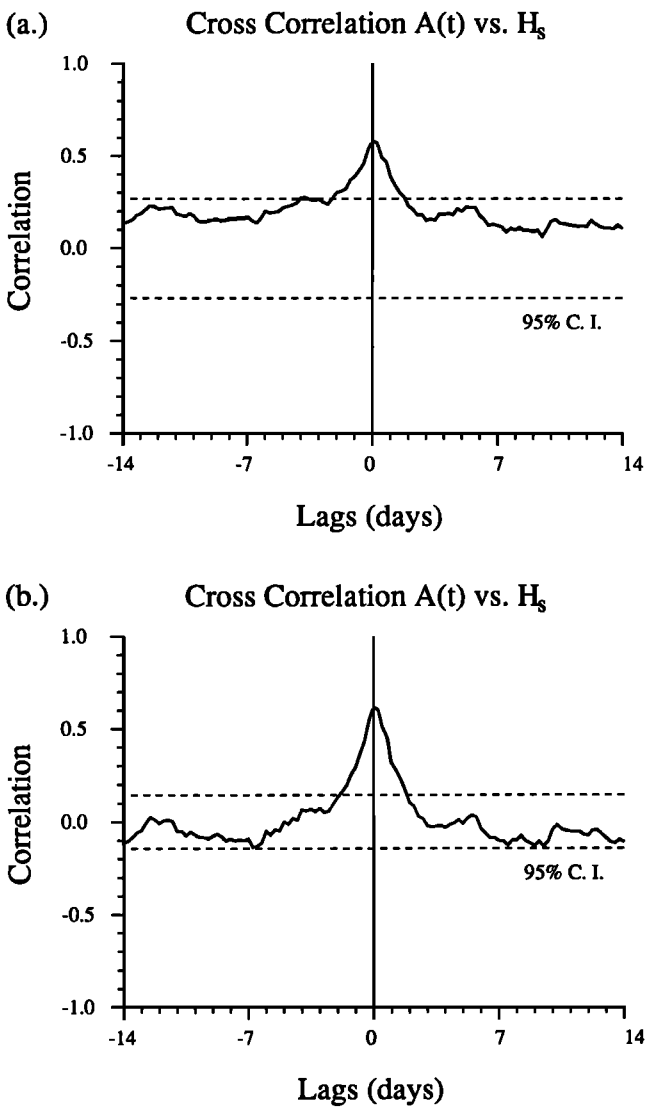

Fig. 11. (*a*) Cross-correlation diagram showing $A(t)$ versus H_s for lags out to ±14 days. (*b*) Same cross-correlations only with each time series detrended with their 21-day means prior to analysis. For each the negative lags indicate H_s leading. The 95% confidence intervals (dashed lines) were calculated using the long-lag artificial skill method [after *Davis*, 1976].

To better emphasize the higher-frequency response of morphology to rapidly changing incident wave conditions associated with storms, cross-correlations between $\Delta A(t)$ and ΔH_s (over a 6-hour period) are computed and shown in Figure 12. The positive correlations from 0 to – 0.5 day lags (r = 0.30–0.37) indicate that changes in wave height tend to precede on-offshore bar migration by less than 1 day, a very rapid response (note that significant correlations at zero lag indicates that changes in each time series occur concurrently). Correlations at all higher lags are observed to be insignificant.

A positive correlation means either that increasing H_s precedes offshore migration or decreasing H_s precedes onshore migration. From this analysis, however, we cannot determine which movement is more important in the correlation. We test the relative contributions of increasing and decreasing wave heights by plotting $\Delta A(t)$ versus $(\Delta H_s)_{max}$ (Figure 13*b*) for the highest correlation (r = 0.48 at zero lag, Figure 13*a*), where $(\Delta H_s)_{max}$ is

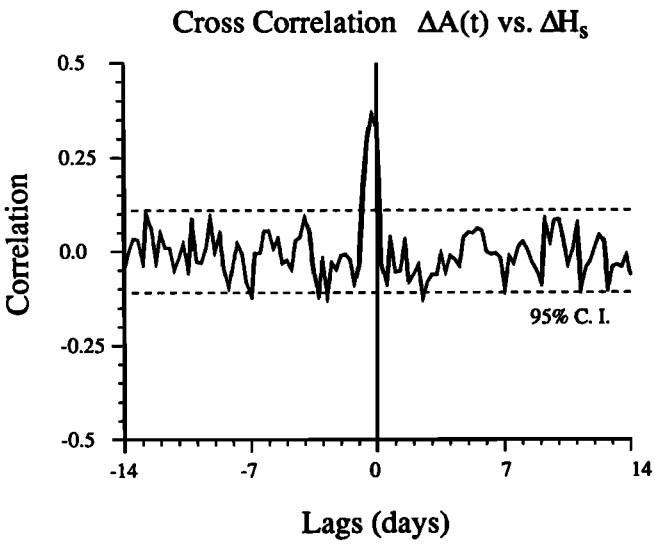

Fig. 12. Cross-correlation diagram showing $\Delta A(t)$ versus ΔH_s for lags out to ±14 days. The negative lags indicate ΔH_s leading. The 95% confidence intervals (dashed lines) were calculated using the long-lag artificial skill method [after *Davis*, 1976].

defined as the largest change in H_s over the preceding 24 hours. These results appear to indicate that the strong significant correlation at zero lag is not dominated by either onshore or offshore migration. However, correlation coefficients for data corresponding to positive $(\Delta H_s)_{max}$ (r = 0.61) are nearly twice as high as for negative $(\Delta H_s)_{max}$ (r = 0.36), indicating that offshore response is more well behaved than onshore response.

Associations between three-dimensional variability and incident wave conditions are investigated with cross-correlations between $V(t)$ and H_s (Figure 14). The negative correlation at zero lag (r = – 0.19) indicates that $V(t)$ is inversely related to incident wave energy. This is consistent with results from the previous section showing that under high waves, bars rapidly become

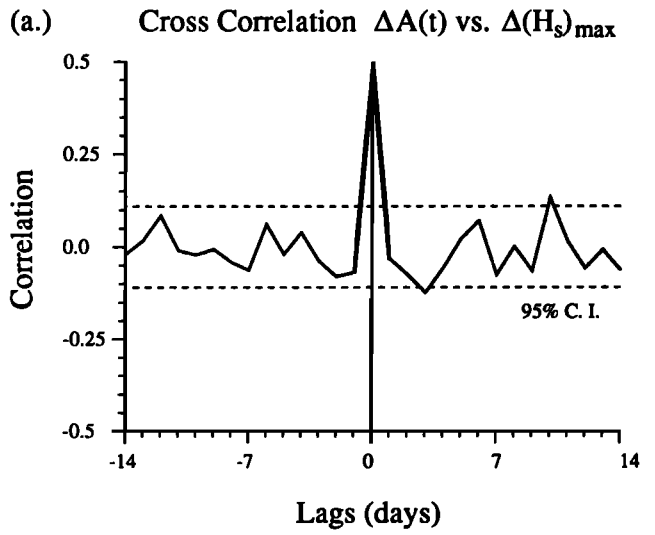

Fig. 13. (*a*) Cross-correlation diagram showing $\Delta A(t)$ versus $(\Delta H_s)_{max}$ for lags out to ±14 days. The negative lags indicate $(\Delta H_s)_{max}$ leading. The 95% confidence intervals (dashed lines) were calculated using the long-lag artificial skill method [after *Davis*, 1976]. (*b*) Plot of $\Delta A(t)$ (abscissa) versus $(\Delta H_s)_{max}$ (ordinate) for the maximum correlation observed at zero lag.

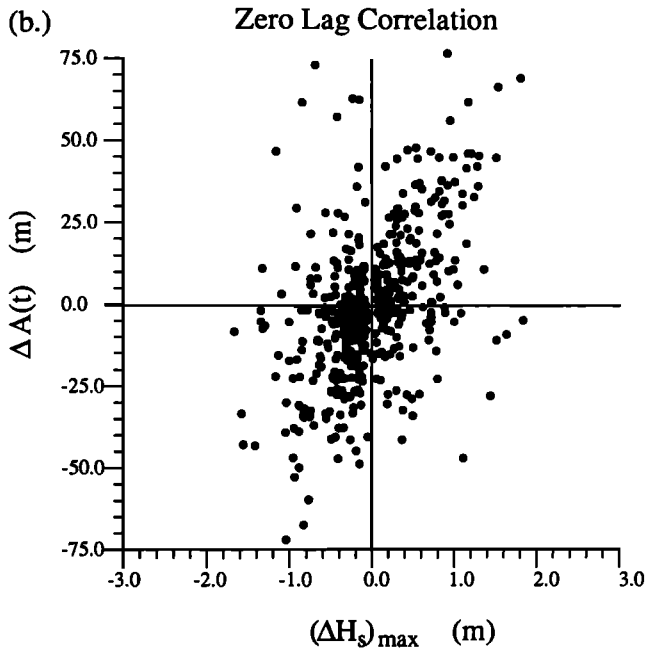

Fig. 13. (continued)

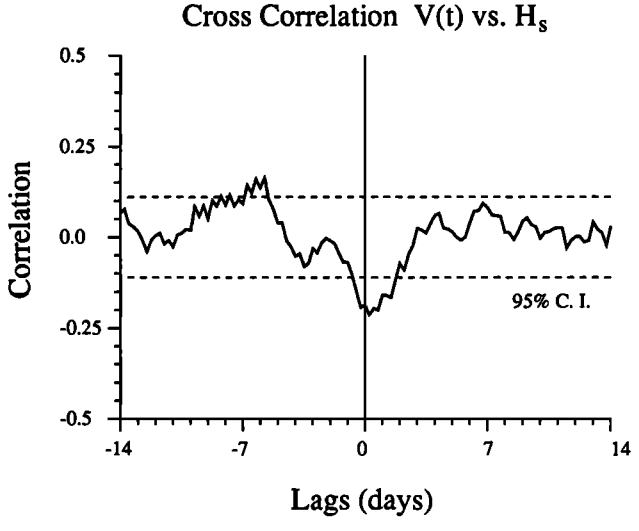

Fig. 14. Cross correlation $V(t)$ versus H_s for lags out to ±14 days. The negative lags indicate H_s leading. The 95% confidence intervals (dashed lines) were calculated using the long-lag artificial skill method [after *Davis*, 1976].

linear. Positive correlations (r = 0.12–0.16) at negative lags associated with H_s leading indicate that large-scale three-dimensional bar structure tends to evolve 5–7 days after large wave events. The negative correlations (r = 0.16–0.21) at short positive lags (less than 2 days) would seem to indicate the nonphysical result that morphology leads incident wave conditions. This result may be qualitatively explained by the observation that the response time scales for offshore, erosive transitions (to more linear morphologic form) under rising wave conditions are much faster than the time scales associated with onshore, accretionary transitions (to more three-dimensional forms). This somewhat puzzling result is the subject of further investigation.

Interestingly, cross-correlations with $\Delta V(t)$ and ΔH_s did not yield significant correlations (Figure 15), nor did analysis with other changes in wave parameters. This is not entirely unexpected, though, considering that evolution of three-dimensionality may involve more complicated processes.

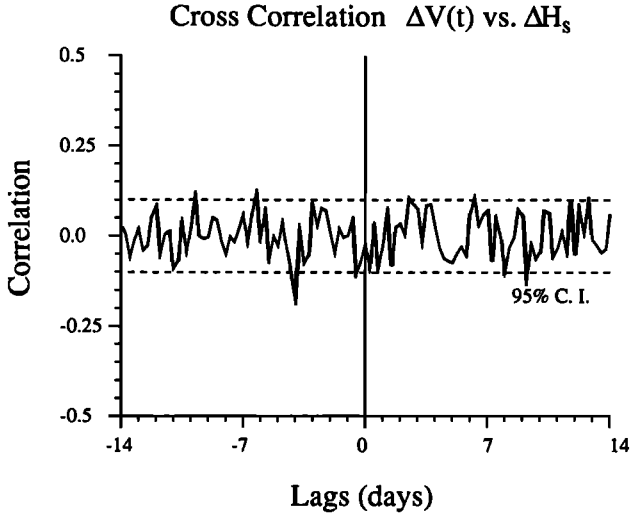

Fig. 15. Cross-correlation $\Delta V(t)$ versus ΔH_s for lags out to ±14 days. The negative lags indicate ΔH_s leading. The 95% confidence intervals (dashed lines) were calculated using the long-lag artificial skill method [after *Davis*, 1976].

Discussion

The bar types defined in the the classification scheme (Figure 1) are unique and encompass the range of possible morphologies from fully dissipative to fully reflective. The model is similar to the previous classification scheme of *Wright and Short* [1984], although derived in a different, independent manner. The most obvious difference is two new bar types which serve to better define longshore variability in bar morphology. These distinctions are valuable when describing bar changes or investigating the formation of longshore variability.

The classification process is made objective by removing as much interpretive bias (associated with visual image analysis) as possible. This is done by defining four basic classification criteria (Table 1) which form a set of discrete, independent decisions that uniquely define each bar type (Figure 3). Some of the decisions, such as the presence of coherent longshore rhythmicity and bar scaling (equations (1) and (2)), may be directly related to processes influencing bar formation [e.g., *Bowen and Inman*, 1971; *Bowen*, 1980; *Holman and Bowen*, 1982] (beyond the scope of this paper).

The parameterization of both the mean cross-shore bar migration (two-dimensional component) and the evolution of longshore variability (three-dimensional component) is successfully accomplished due to the quantitative nature of the time exposure technique in estimating bar crest position. As an analytic method, empirical orthogonal functions work because the data mean is linear (and homogeneous alongshore) and one spatial factor (in this case the first) is linear, thus isolating the variance of the mean cross-shore movement.

We find that the development of two-dimensional morphology (no longshore variability) occurs very rapidly following increases in wave energy, on the order of less than 1 day, the same as time

scales of change for incident wave conditions. Initial transition from linear to three-dimensional morphology occurs as wave height decreases, also on the same time scale as the waves. Conversely, transitions to lower states occur on longer time scales than wave decay. Classification analysis of morphology shows that initial formation of longshore variability may be quite rapid, commonly less than 1 day after the peak of high wave events. Continued periods of low wave energy generally result in the formation of large-scale three-dimensionality, with time scales of 5–7 days, much longer than time scales of wave decay, consistent with recent short-term field results [*Sallenger et al.*, 1985; *Howd and Birkemeier*, 1987*b*).

A more accurate estimation of the time scale for initial formation of three-dimensionality is not possible with this data set (since our maximum morphologic resolution is 1 day). We find that changes in wave height do not correlate (at the 95% significance level) with the formation of longshore variability. This is not unexpected considering the complex dynamical processes thought to be important in controlling nearshore topography. It is interesting to note, though, that coherent longshore structure observed in bars typically has very large length scales on the order of hundreds of meters, lending support to models incorporating low-frequency (infragravity band) motions with similar length scales (equations (1) and (2)).

Transitional sequences observed in the data indicate that progression down the model from higher to lower bar types occurs sequentially and is associated with lower wave conditions, thus representing an accretional (onshore) progression. Under rising wave conditions, transitions are more evenly spread among possible higher states, representing an erosional (offshore) progression. This indicates the important result that up-state, erosional transitions appear to occur with time scales of change of incident wave energy, favoring equilibrium modeling; under accretional conditions, transitions tend to be more dependant on preceding morphology than on local wave height, with time scales of change much longer than the waves, favoring sequential modeling. The dependence of onshore, accretional transitions on preceding morphology was also noted by *Wright et al.* [1985]. Thus, morphology data support two types of bar generation models, sequential and equilibrium, under different conditions.

Morphology correlates best with simple offshore wave height. The correlation is primarily a result of storm events, which characterize the incident wave climate much of the year. This is somewhat inconvenient, though, since nondimensional surf similarity parameters, such as the Iribarren number, allow for easier comparisons with other field sites.

The transition from a linear to a longshore variable morphology is of particular interest in addressing bar genesis. In the past, quantifying linearity in bar form has proved to be an arduous task, exacerbated by the difficulty in defining bar morphology under adverse conditions. With our sampling technique, linear bars (as well as longshore variable bars) are relatively easy to identify under all wave conditions (provided breaking occurs over the bar). Our observations show that linear bars (Bar Type G) tend to occur exclusively during storm periods; furthermore, during the peak of storms the most commonly occurring morphology is linear. Rapid development of three-dimensional structure follows the decline of wave energy, indicating that linear bars are unstable ($\langle\tau_G\rangle \approx 2$ days) and are only maintained under high waves, shown by both characterization methods.

Nonrhythmic bars are also transient ($\tau_C \approx \tau_F \approx 3$ days), irrespective of shoreline attachment points. These bars occur under a wide range of conditions, although they are usually associated with a change in wave height, suggesting that this morphology is also very unstable. Those with continuous troughs (Bar Type F) generally occur immediately after linear bars and prior to the formation of dominant longshore periodicity, suggesting that they fit a natural progression between differing levels of three-dimensionality. Conversely, those with shore attachments (Bar Type C) do not appear to fit regular sequences, suggesting that the processes controlling this morphology are unclear.

The formation of longshore rhythmicity has major implications in bar evolution and has been a primary objective of intensive short-term field studies focused on single storm events [*Sallenger et al.*, 1985; *Howd and Birkemeier*, 1987*b*]. We observe rhythmic bars (Bar Types D and E) to occur typically 5–16 days following the peaks of storms, though response times may be much quicker (on the order of 1–2 days). Once well-developed, they tend to be very stable under moderate waves, with residence times increasing with proximity to the shoreline ($\tau_E \approx 5$ days, $\tau_D \approx 11$ days). This is observed in bars that maintain their longshore structure when slowly migrating onshore under low waves, but rapidly degrading with onset of high waves (also observed by *Wright et al.* [1985]). Rhythmic bars (most often crescentic bars) are very common at this field site, indicating that this morphology may be the preferred morphologic configuration.

The results are clear in their indication that long records are invaluable in assessing the morphologic behavior of sand bars. Predictability is not likely using just incident wave parameters, although a general understanding of transitional sequences with respect to large storm events is possible with long data records. Short-term intensive experiments investigating other fluid motions (such as edge waves) are necessary to address bar genesis. This study presents evidence that these experiments should be concentrated around storm events when three-dimensional bar morphology is rapidly evolving.

Special mention concerning errors in the time series, $A(t)$ and $V(t)$, arising from tidal fluctuations (mentioned earlier) is appropriate, since this is the first instance the time exposure technique has been applied over an extended period. As expected, the time series show a systematic correlation (though not significant for 95% confidence) resulting from tidal fluctuations (aliased into a ~15 day period) affecting our bar position estimate [LH89]. This signal would appear to increase the variance of $A(t)$; however, discrepancies in offshore bar crest estimations (away from the true position) are not solely the result of the tide. Since the tide does not change dramatically between day-to-day samples (taken at approximately the same time), most short-term variation (order of 1–2 days) in the data is associated with changing incident wave height. Therefore, removing the insignificant systematic long-lag correlations would inevitably result in the introduction of significant tidal contamination at zero lag, the time scale of highest interest. Hence, our main concern is associated with the maximum offshore discrepancy. This magnitude was estimated by regressing $A(t)$ against the measured tidal signal (relative to mean sea level), and found to be 13.5 m, within our estimated error for the technique (~15 m).

$V(t)$ also shows an apparent systematic signal associated with tidal fluctuations. We note, though, that the nature of this noise is not the same as for $A(t)$. The effect of the tide on the estimation of longshore bar variability is explained in LH89. The major point is that at lower water levels, maximum wave dissipation occurs further offshore where longshore variability of contours may be less. This could serve to reduce the estimated longshore variance in bar crest position, and would tend to have higher effects at

lower water levels [LH89]. However, our main interest is with changes over short time scales (order of days), much less than the aliased tidal signal (~15 days), and so the effect on longshore variability estimation is minimized.

CONCLUSIONS

A 2 year dataset of daily sand bar morphology estimates has been collected on a naturally barred beach at Duck, N.C. Daily time exposure images allow improved assessment of overall morphology as well as quantitative estimates of bar crest position as a function of longshore location. Significant wave height and peak period data provided environmental control. Analyses follow two lines. First, bar samples are visually identified using four morphologic classification criteria. Second, using empirical orthogonal functions (EOFs), the variability in bar structure is split into two-dimensional (linear) and three-dimensional (longshore variable) components.

A new eight-bar-type classification scheme is presented that represents the morphologic variability of nearshore sand bars observed at the field site. The scheme is consistent with previous work and, in particular, compares well with the most highly evolved classification model of *Wright and Short* [1984]. Four classification criteria are chosen, each of which may be related to processes associated with models of bar generation. The classification provides a complete set of morphologic bar types in which each state is defined uniquely (every beach morphology is described by one and only one state). Calibration studies show that operator subjectivity is small.

The most common bar form is longshore-periodic (rhythmic) bars observed in 68% of the data. Analysis reveals that linear bars occur under highest wave conditions ($\bar{H}_s$ = 1.78 m) and are unstable (mean residence time ≈ 2 days), whereas shore-attached crescentic bars are the most stable (mean residence time ≈ 11 days) and generally form 5–16 days following peak wave events. Non-rhythmic, three-dimensional bars are very transient (mean residence time ≈ 3 days). The classification scheme shows qualitatively good correlations between bar type transitions and incident wave parameters.

The ordering of the bar types yields a good first-order approximation of accretional (offshore bar migration) and erosional (onshore bar migration) sequences. Transitions to progressively more stable bars generally occur sequentially (87%) under declining wave conditions, while transitions to higher states are more evenly spread among possible higher bar types and occur under rising wave energy, with higher jumps in state resulting from larger increases in wave energy. Thus, the data support two types of bar generation models. Up-state, erosional transitions are more closely related to equilibrium conditions associated with incident wave energy, and for down-state, accretional transitions the bar behaves in a sequential manner with greater dependence on preceding morphology than on local wave height.

Bar samples are also digitized to yield quantitative estimates of bar crest position and longshore variability. Principal component analysis was used to decompose the data into two-dimensional (linear) and three-dimensional (longshore variable) components. Cross-shore bar migration dominates bar variability (accounting for 74.6% of the variance) and rapidly responds to changing wave conditions (with time scales less than 1 day). Longshore bar structure accounts for ~14% of the variance, where the remaining variance is associated with errors, partly a result of tidal contamination arising from the sampling technique. Three-dimensional bar structures evolve rapidly, with changes in longshore variability inversely related to changing wave conditions. The evolution to coherent longshore periodicity occurs 5–7 days following the peak of high-energy storm events.

Acknowledgments. We would like to thank the entire FRF staff for graciously collecting the video and wave data, particularly Bill Birkemeier and the many people in the "Infragravity Waves in the Nearshore Zone" work unit headed by Kent Hathaway. Joan Oltman-Shay, Paul Komar, and Pete Howd provided critical review and enhanced many stimulating discussions. The following individuals tested the classification process and we thank them for their consideration and conscientious efforts: Joan Oltman-Shay, Pete Howd, Todd Holland, Mark Lorang, Jim Tait, John Marra, and Zhenlin Li. Further acknowledgement is extended to the reviewers for their thorough and insightful comments which greatly improved the paper. Also, thanks to Marcia Turnbull for typesetting the final manuscript, and to Vicki Lorang for drafting a number of the figures. Funding for the project was provided by the Office of Naval Research, Coastal Sciences Program, under contract N00014-84-0218, and by the U.S. Army Corps of Engineers, Coastal Engineering Research Center under the Barrier Island Sedimentation work unit. Finally, thanks to Ralph Miller for the 2-2-1 full court press.

REFERENCES

Aubrey, D. G., Seasonal patterns of onshore/offshore sediment movement, *J. Geophys. Res.*, *84*, 6347–6354, 1979.

Aubrey, D. G., and R. M. Ross, The quantitative description of beach cycles, *Mar. Geol.*, *69*, 155–170, 1985.

Aubrey, D. G., D. L. Inman, and C. D. Winant, The statistical prediction of beach changes in southern California, *J. Geophys. Res.*, *85*, 3264–3276, 1980.

Birkemeier, W. A., Time scales of nearshore profile change, in *Proceedings of the 19th International Conference on Coastal Engineering*, pp. 1507–1521, American Society of Civil Engineers, New York, 1985.

Birkemeier, W. A., H. C. Miller, S. D. Wilhelm, A. E. DeWall, and C. S. Gorbics, User's guide to CERC's Field Research Facility, Instruction Report-85-1, Coastal Eng. Res. Cent., Field Res. Facil., U. S. Army Eng. Waterw. Exp. Sta., Vicksburg, Miss., 1985.

Birkemeier, W. A., C. F. Baron, M. W. Leffler, H. C. Miller, J. B. Strider, and K. K. Hathaway, SUPERDUCK nearshore precesses experiment: Data summary, miscellaneous reports, Coastal Eng. Res. Cent., Field Res. Facil., U.S. Army Eng. Waterw. Exp. Sta., Vicksburg, Miss., 1989.

Bowen, A. J., Simple models of nearshore sedimentation: Beach profiles and longshore bars, Coastline of Canada, Littoral Processes and Shore Morphology, *Geol. Surv. Can. Pap.*, *80–10*, 1–11, 1980.

Bowen, A. J., and D. L. Inman, Edge waves and crescentic bars, *J. Geophys. Res.*, *76*, 8662–8671, 1971.

Carter, T. G., P. L. Liu, and C. C. Mei, Mass transport by waves and offshore sand bedforms, *J. Waterw. Harbors Coastal Eng. Div., Am. Soc. Civ. Eng.*, *WW2*, 165–184, 1973.

Chappell, J., and I. G. Eliot, Surf-beach dynamics in time and space—an Australian case study, and elements of a predictive model, *Mar. Geol.*, *32*, 231–250, 1979.

Crowson, R. A., W. A. Birkemeier, H. M. Klein, and H. C. Miller, SUPERDUCK nearshore processes experiment: Summary of studies, technical report, Coastal Eng. Res. Cent., Field Res. Facil., U.S. Army Eng. Waterw. Exp. Sta., Vicksburg, Miss., 1988.

Davis, R. E., Predictability of sea surface temperature and sea level pressure anomalies over the North Pacific Ocean, *J. Phys. Oceanogr.*, *6*, 249–266, 1976.

Dean, R. G., Heuristic models of sand transport in the surf zone, Proceedings of the International Conference on Coastal Engineering Dynamics in the Surf Zone, Sydney, N. S. W., 208–214, 1973.

Goldsmith, V., D. Bowman, and K. Kiley, Sequential stage development of crescentic bars: Hohaterim beach, southeastern Mediterranean, *J. Sediment. Petrol.*, *52*, 233–249, 1982.

Gourlay, M. R., Beach and dune erosion tests, *Rep. M935/M936*, Delft Hydraulics Laboratory, Delft, Netherlands, 1968.

Greenwood, B., and R. G. D. Davidson-Arnott, Marine bars and nearshore sedimentary processes, Kouchibouguac Bay, New Brunswick, Canada, in *Nearshore Sediment Dynamics and Sedimentation*, pp. 123–150, John Wiley, New York, 1979.

Holman, R. A., and A. J. Bowen, Bars, bumps, and holes: Models for the

generation of complex beach topography, *J. Geophys. Res.*, *87*, 457–468, 1982.

Howd, P. A., and W. A. Birkemeier, Beach and nearshore survey data: 1981–1984, *Tech. Rep. 87–89*, Coastal Eng. Res. Cent., Field Res. Facil., U.S. Army Eng. Waterw. Exp. Sta., Vicksburg, Miss., 1987*a*.

Howd, P. A., and W. A. Birkemeier, Storm induced morphology changes during DUCK85, in *Proceedings of Coastal Sediments '87*, pp. 834–847, American Society of Civil Engineers, 1987*b*.

Hunt, I. A., Design of seawalls and breakwaters, *Proc. Am. Soc. Civ. Eng.*, *85*, 123–152, 1959.

Keulegan, G. H., An experimental study of submarine sand bars, *Tech. Memo. 3*, 40 pp., U.S. Army Corps of Eng., Beach Erosion Board, 1948.

Lau, J., and B. Travis, Slowly varying Stokes waves and submarine longshore bars, *J. Geophys. Res.*, *78*, 4489–4497, 1973.

Lippmann, T. C., and R. A. Holman, Quantification of sand bar morphology: A video technique based on wave dissipation, *J. Geophys. Res.*, *94*, 995–1011, 1989.

Mason, C., W. A. Birkemeier, and P. A. Howd, Overview of DUCK85 nearshore processes experiment, in *Proceedings of the 20th International Conference on Coastal Engineering*, pp. 818–833, American Society of Civil Engineers, New York, 1987.

Miller, H. C., W. A. Birkemeier, and A. E. DeWall, Effects of CERC research pier on nearshore processes, in *Proceedings of the International Conference on Coastal Structures '83*, pp. 765–782, American Society of Civil Engineers, New York, 1983.

Miller, R. L., Role of vortices in surf zone prediction: Sedimentation and wave forces, beach and nearshore sedimentation, *Spec. Publ. Soc. Econ. Paleontol. Mineral.*, *24*, 92–114, 1976.

Priesendorfer, R. W., F. W. Zwiers, and T. P. Barnett, Foundations of principal component selection rules, *SIO Rep. 81–4*, 200 pp., Scripps Inst. of Oceanogr., La Jolla, Calif., 1981.

Sallenger, A. H., R. A. Holman, and W. A. Birkemeier, Storm induced response of a nearshore bar system, *Mar. Geol.*, *64*, 237–257, 1985.

Shepard, F. P., Longshore bars and troughs, *Tech. Memo. 15*, 31 pp., U.S. Army Corps of Eng., Beach Erosion Board, 1950.

Short, A. D., Multiple offshore bars and standing waves, *J. Geophys. Res.*, *80*, 3838–3840, 1975.

Short, A. D., Three-dimensional beach stage model, *J. Geol.*, *87*, 553–571, 1979.

Sonu, C. J., Three-dimensional beach changes, *J. Geol.*, *81*, 42–64, 1973.

Sonu, C. J., and W. R. James, A Markov model for beach profile changes, *J. Geophys. Res.*, *78*, 1462–1471, 1973.

Sonu, C. J., and J. L. van Beek, Systematic beach changes on the Outer Banks, North Carolina, *J. Geol.*, *79*, 416–425, 1971.

Sunamura, T., Beach morphologies and their change, in *Nearshore Dynamics and Coastal Processes: Theory, Measurement, and Predictive Models*, pp. 136–152, University of Tokyo Press, Tokyo, 1988.

Ursell, F., Edge waves on a sloping beach, *Proc. R. Soc. London, Ser. A*, *214*, *79*, 1952.

Wright, L. D., and A. D. Short, Morphodynamics of beaches and surf zones in Australia, in *CRC Handbook of Coastal Processes and Erosion*, pp. 35–64, CRC Press, Boca Raton, Fla., 1983.

Wright, L. D., and A. D. Short, Morphodynamic variability of surf zones and beaches: A synthesis, *Mar. Geol.*, *56*, 93–118, 1984.

Wright, L. D., J. Chappell, B. G. Thom, M. P. Bradshaw, and P. Cowell, Morphodynamics of reflective and dissipative beach and inshore systems: Southeastern Australia, *Mar. Geol.*, *32*, 105–140, 1979.

Wright, L. D., A. D. Short, and M. O. Green, Short-term changes in the morphodynamic states of beaches and surf zones: An empirical predictive model, *Mar. Geol.*, *62*, 339–364, 1985.

Wright, L. D., P. Nielsen, N. C. Shi, and J. H. List, Morphodynamics of a bar trough surf zone, *Mar. Geol.*, *70*, 251–285, 1986.

R. A. Holman and T. C. Lippmann, College of Oceanography, Oregon State University, Corvallis, OR 97331.

(Received March 31, 1989;
accepted October 13, 1989.)